PERGAMON

International Journal of Solids and Structures 39 (2002) 3373–3386

INTERNATIONAL JOURNAL OF SOLIDS and STRUCTURES

www.elsevier.com/locate/ijsolstr

Numerical analysis of buckling-driven delamination

H.M. Jensen *, I. Sheinman [1]

Department of Solid Mechanics, Technical University of Denmark, Building 404, DK-2800 Lyngby, Denmark

Received 13 February 2002

Abstract

Conditions for steady-state growth of buckling-driven delamination in thin film systems can be calculated by a simplified method where details around the growing front are not required. The simplified method relies upon estimates of the phase angle of loading along the propagating front of delamination and the accuracy of these estimates are investigated by comparing with finite element calculations of the fracture mechanics parameters along the growing front. The sensitivity of the parameters to the shape of the front is investigated and it is shown that the simplified approach for estimating the phase angle of loading on the growing front of delamination is very accurate. A comparison is made between steady-state delamination growth along circular paths of different curvatures but with identical widths so that the phase angle of loading on the growing front can be assumed to be the same independent of the curvature.

Keywords: Propagating instabilities; Buckling-driven delamination; Mixed mode interface fracture; Thin film systems; Layered materials

1. Introduction

Delamination of thin films or layers by a mechanism, where buckling of the film coupled with interface cracking grows in a self-similar fashion, is recognised as an important failure mode (Wang and Evans, 1998). The buckling-driven delamination is sketched in Fig. 1: a film of thickness h is bonded to a substrate. The bonded film is subject to equi-biaxial compressive stresses—usually due to the manufacturing process—and these are assumed homogeneous throughout the bonded film. From an initial flaw at the interface, the compressive stresses cause buckling of the film. The boundary between the bonded and the delaminated coating is treated as an interface crack front which is unloaded prior to buckling and loaded in combined mode I, II and III after buckling.

The delamination grows along the curved front leaving behind arrested cracks along the sides. The stress state far behind the growing crack front will be independent of the co-ordinate in the growth direction. If the curved front grows along a linear path, the cracks left behind will be straight-sided. The in-plane extent

* Corresponding author. Fax: +45-45-93-14-75.
E-mail address: henrik@fam.dtu.dk (H.M. Jensen).
[1] Permanent address: Department of Civil Engineering, Technion—Israel Institute of Technology, Haifa 32000, Israel.

0020-7683/02/$ - see front matter
PII: S0020-7683(02)00158-0

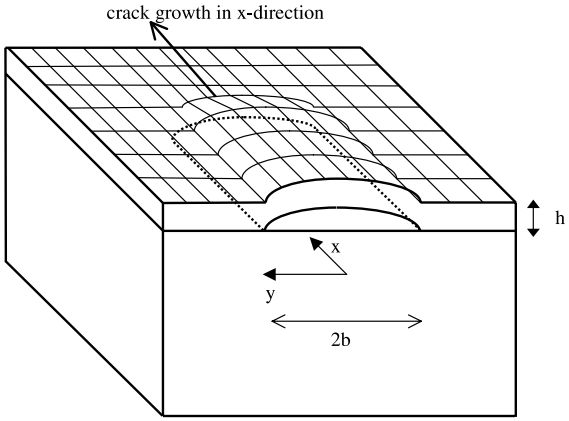

Fig. 1. Schematic illustration of straight-sided buckling driven delamination. The film above the delamination buckles away from the substrate and the front of delamination grows along a linear path.

of delamination, $2b$, is assumed to be large compared to h. This allows the energy release rate and the stress intensity factors to be calculated by two uncoupled problems: the stresses and deformations in the delaminated film are found by geometrical non-linear plate theory taking the film to be clamped to the substrate along the crack front, and the discontinuities of stresses across the crack front obtained by this analysis is coupled to local fracture mechanics solutions for the J-integral and phase angles of loading.

The buckling-driven delamination mode growing along a linear path has been observed in thermal barrier coatings (Sergo and Clarke, 1998), in solar cells (Thouless, 1993) and in model systems (Thouless et al., 1992).

Other buckling-driven delamination modes observed experimentally—for instance in systems with hard coatings—include a mode, which leaves wavy sides behind the growing front (e.g. Matuda et al., 1981; Gille and Rau, 1984; Ogawa et al., 1986; Thouless et al., 1992; Thouless, 1993; Iyer et al., 1995). The straight-sided delamination mode have been applied in such cases as an approximate, qualitative model, while Ortiz and Gioia (1994) and Gioia and Ortiz (1996) have formulated more rigorous models applying to such delamination modes. The straight-sided mode of delamination is applied also in Hutchinson (2000) to study effects of substrate curvature and in Hutchinson et al. (2000) to study effects of imperfections such as non-planar interfaces.

The analyses of buckling-driven delamination (Hutchinson and Suo, 1992; Choi et al., 1999) utilise the steady-state nature of the buckle propagation. A scheme is formulated, which allows the energy release rate along the growing crack front to be calculated by considering only stresses in the delaminated film far behind the front. There, the stresses are independent of the co-ordinate in the direction of crack growth and as a result the governing equations for the steady-state energy release rate can be solved in closed form. The expression is exact and thus details of the shape of the growing front and variations of stress intensity factors along the front would not be needed if the fracture criterion depends only on the energy release rate. This is not the case, however, for buckling-driven delamination where the crack tip loading is mode II dominated, and experimental results have demonstrated a very significant effect of the phase angle of loading for interface cracks on the fracture toughness (Cao and Evans, 1988). The phase angle of loading depends on the shape of the growing front and in order to estimate it, Hutchinson and Suo (1992) and Choi et al. (1999) suggested various schemes based on solutions for a full circular delamination.

In the present work at first finite element calculations are carried out resolving details along the growing interface crack front. A sketch of the buckling-driven delamination seen perpendicular to the interface is shown in Fig. 2. The symmetry conditions with respect to both the x- and the y-axis are utilised in the finite

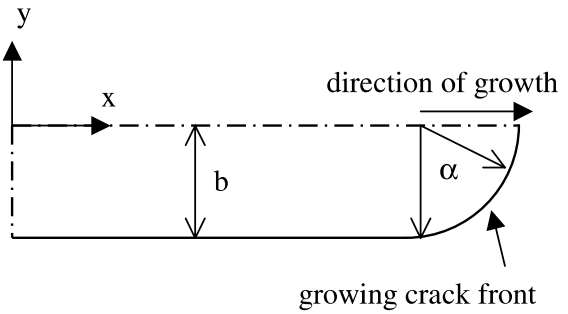

Fig. 2. The straight-sided delamination seen from above. Symmetry with respect to both the x- and the y-axis is utilised. The angle α specifies the location along the growing front.

element calculations. A comparison of the finite element results with results based on the scheme proposed by Choi et al. (1999) is carried out in order to assess the accuracy of the simplified model. The steady-state energy release rate required for growth along a linear path is then compared with the energy release rate required for growth along a circular path. The results provide insight into possible mechanisms causing buckling-driven delamination along wavy or curved paths to be more common at high residual stress levels than delaminations growing along a linear path.

2. Fracture mechanics of delamination

The energy release rate, G, along a crack between a thin film and a substrate can be calculated by the normal membrane stress, ΔN, the shear membrane stress, ΔT, and the bending moment, M, in the film at the crack (Jensen et al., 1990; Suo and Hutchinson, 1990) as

$$G = G_{\mathrm{I/II}} + G_{\mathrm{III}}, \quad G_{\mathrm{I/II}} = \frac{1-\nu^2}{2Eh^3}\left(12M^2 + h^2\Delta N^2\right), \quad G_{\mathrm{III}} = \frac{1}{2\mu h}\Delta T^2 \tag{1}$$

where E and ν are the Young's modulus and Poisson's ratio for the film, and μ is the elastic shear modulus. Delaminations of relatively large extent compared to the film thickness, h, are assumed so that effects due to the curvature of the crack front and inhomogeneous stress states can be neglected.

It has been observed experimentally that interface fracture toughness is significantly influenced by the ratios between the stress intensity factors (e.g. Cao and Evans, 1989). For this reason a decomposition of the energy release rate into mode I, II and III stress intensity factors, K_{I}, K_{II}, K_{III}, is required which involves the elastic properties of the substrate, E_{s}, ν_{s} and μ_{s}. The phase angles of loading, ψ and ϕ, introduced in Rice (1988), Suo and Hutchinson (1990) and Jensen et al. (1990) give a such decomposition:

$$\tan\psi = \frac{K_{\mathrm{II}}}{K_{\mathrm{I}}} = \frac{\sqrt{12}M\cos\omega + h\Delta N\sin\omega}{-\sqrt{12}M\sin\omega + h\Delta N\cos\omega}, \quad \cos\phi = \sqrt{\frac{G_{\mathrm{III}}}{G}} \tag{2}$$

Here, ω has been tabulated in Suo and Hutchinson (1990) as a function of the elastic mismatch in the bimaterial system. Eq. (2) holds in the special case of non-oscillating crack tip singularities and such bimaterial combinations are considered below. By (2) it is seen that $\psi = 0°$ under pure mode I loading conditions and $\psi = \pm 90°$ under pure mode II load conditions. The methods used and most results hold also for oscillating singularities provided the size of the contact region close to the crack tip is small compared to the film thickness. Due to the assumptions mentioned the deformations and stresses in the delaminated

region can be determined by plate theory. Cases where the film and the substrate overlap can be prevented within this theory by enforcing contact conditions. There are, however, cases such as those investigated in Stringfellow and Freund (1993) where large-scale contact effects cannot be resolved by simple plate theory, but rather require solution of the full elasticity equations. The effect of large-scale contact in such cases should be included via the interface fracture criterion in the present formulation. For this analysis it is believed that no essential features result from oscillating crack tip singularities. The first Dundurs' parameter (Dundurs, 1969) is defined as

$$\alpha_{\mathrm{D}} = \frac{\frac{E}{1-\nu^2} - \frac{E_{\mathrm{s}}}{1-\nu_{\mathrm{s}}^2}}{\frac{E}{1-\nu^2} + \frac{E_{\mathrm{s}}}{1-\nu_{\mathrm{s}}^2}} \tag{3}$$

The relationship between the energy release rate and the stress intensity factors is

$$G = \frac{K_{\mathrm{I}}^2 + K_{\mathrm{II}}^2}{2}\left(\frac{1-\nu^2}{E} + \frac{1-\nu_{\mathrm{s}}^2}{E_{\mathrm{s}}}\right) + \frac{K_{\mathrm{III}}^2}{4}\left(\frac{1}{\mu} + \frac{1}{\mu_{\mathrm{s}}}\right) \tag{4}$$

and by combination of (1), (2) and (4) the stress intensity factor are obtained as

$$K_{\mathrm{I}} = -\left(\frac{\Delta N}{\sqrt{2h}}\cos\omega - M\sqrt{\frac{6}{h^3}}\sin\omega\right)\sqrt{1-\alpha_{\mathrm{D}}}, \quad K_{\mathrm{II}} = K_{\mathrm{I}}\tan\psi, \quad K_{\mathrm{III}} = \Delta T\sqrt{\frac{2}{h}}\sqrt{\frac{1}{1+\mu/\mu_{\mathrm{s}}}} \tag{5}$$

with $\tan\psi$ given in (2).

3. Steady-state growth of straight-sided delamination

Assume a delamination of width $2b$ propagating along a line as sketched in Fig. 2. Provided the energy released during delamination growth is load-path independent the energy release rate along the growing front, G_{ss}, is (Hutchinson and Suo, 1992)

$$G_{\mathrm{ss}} b = \int_0^b G_{\mathrm{side}}(\tilde{b})\,\mathrm{d}\tilde{b} \tag{6}$$

where the energy release rate along the sides of a straight-sided delamination far behind the propagating front, G_{side}, can be obtained by a simplified, one-dimensional analysis where details along the curved propagating delamination front are not required.

The exact solution to the von Karman equations of a clamped/clamped strip of unit width undergoing x-independent deformation and loaded by thermal contraction of the substrate gives the following discontinuities of membrane force and bending moment across the crack front (Hutchinson and Suo, 1992; Jensen, 1993)

$$\frac{12(1-\nu^2)\,\Delta N b^2}{Eh^3} = \pi^2\left(\frac{\sigma}{\sigma_{\mathrm{c}}} - 1\right), \quad \frac{12(1-\nu^2)Mb^2}{Eh^4} = \frac{\pi^2}{\sqrt{3}}\sqrt{\frac{\sigma}{\sigma_{\mathrm{c}}} - 1} \tag{7}$$

provided the equi-biaxial stress, σ, in the bonded film exceeds the bifurcation stress, σ_{c}, given by

$$\sigma_{\mathrm{c}} = \frac{\pi^2 E h^2}{12(1-\nu^2)b^2} \tag{8}$$

Finally, by (1), and (6)–(8)

$$G_{\mathrm{side}} = G_0\left(1 - \frac{\sigma_{\mathrm{c}}}{\sigma}\right)\left(1 + 3\frac{\sigma_{\mathrm{c}}}{\sigma}\right), \quad G_{\mathrm{ss}} = G_0\left(1 - \frac{\sigma_{\mathrm{c}}}{\sigma}\right)^2, \quad G_0 = \frac{\sigma^2(1-\nu^2)h}{2E} \tag{9}$$

A Griffith fracture criterion based on G_{ss} would be inadequate since ψ is close to $-90°$ for buckling-driven delamination (Hutchinson and Suo, 1992) and experimental results show a very significant dependence of the interface fracture toughness on ψ (Cao and Evans, 1989). Furthermore, G_{side} is always larger than G_{ss} indicating (with a Griffith fracture criterion imposed) that growth would always take place along the sides rather than at the front, which would be in disagreement with observations. Also G_{ss} is a monotonically increasing function of the width, $2b$, of delamination indicating (again with a Griffith fracture criterion imposed) that a characteristic width of delamination would not exist since more energy would be released with a greater width. Also this would be in disagreement with observations where delaminations grow with a characteristic width. For the reasons mentioned it is then clear that the phase angle of loading at the growing crack front is required in the analysis.

The estimate of the phase angle of loading at the growing front, which has been suggested by Choi et al. (1999) is to take ψ for a full circular blister with radius equal to b at a residual stress where the energy release rate is equal to G_{ss}. The numerical solution for the full circular blister simplifies since the deformation is axi-symmetric. The purpose of the finite element calculations in Section 4 is to investigate the accuracy of the scheme for estimating ψ.

By (9) it is seen that G_{side} and G_{ss} both converge to G_0 as the normalised stress tends to infinity corresponding to the width of the delamination becoming infinitely large. This limit value of the energy release rate corresponds to the energy stored in the film being released under plane strain conditions (Hutchinson and Suo, 1992). This energy is considerably lower than the total energy stored in the film, G_1, which is given by

$$G_1 = \frac{\sigma^2(1-\nu)h}{E} \tag{10}$$

The purpose of the comparison between steady-state energy release rates for straight-sided and curved delaminations in Section 5 is to investigate whether other delamination modes than the straight-sided may release a larger portion of the energy stored in the film.

4. Finite element calculations

The straight-sided mode of delamination sketched in Fig. 2 is analysed numerically by the finite element method in the following. Symmetry with respect to the x- and y-axis is assumed. Bifurcation buckling into non-symmetric deformation with respect to the x-axis was investigated in Jensen and Sheinman (2001). The length of the straight-sided segment behind the propagating front is taken to be $3b$. Results are obtained assuming elliptic shapes of the growing front. The finite element calculations are based on the finite element code ADINA (ADINA, 1994). The elements chosen in the calculations are seven-noded triangular elements, which in comparison with other elements resolve the stress resultants along the boundary with higher accuracy. Results are compared for two mesh sizes: one with 960 elements and one with 1500 elements. The comparison shows only minor differences for the circular shape of the growing front, but increasing differences between calculations based on the two meshes show up as the shape becomes elliptic with the largest semi-axis in the x-direction. In the calculations, $\nu = 0.2$ has been used. A small imperfection of the shape of the delaminated region normal to the interface is assumed to initiate out-of-plane deformation. Non-linearities resulting from large deformations of the delaminated region compared to h (but assuming moderate rotations) are retained in the governing equations. The equilibrium path is traced by increasing the residual stress or the normal deformation incrementally and performing equilibrium iterations. The stress discontinuities computed across the crack front are coupled to (1), (2) and (6) using $\omega = 52.1°$ corresponding to the case of no elastic mismatch between the film and the substrate. Note, that different elastic constants of the film and the substrate would just require changing α_D and ω in (2) and (6).

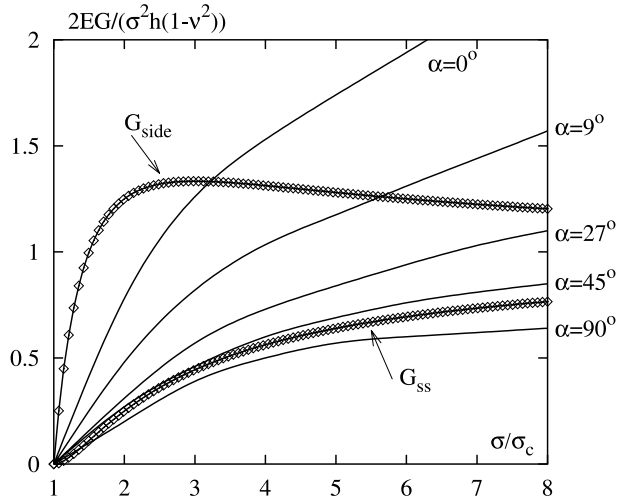

Fig. 3. Variation of energy release rate with increasing residual stresses shown at different locations along a circular crack front.

In Fig. 3 results for the energy release rate calculated numerically at various angles, α (shown in Fig. 2), along the growing front have been compared with the exact results for G_{side} and G_{ss} (9). The energy release rate in the region around the transition between the growing front and the unloaded crack left behind (α close to 0) has a high peak. This peak is quite sensitive to the curvature of the growing front in that region. The peak value of G decreases as the curvature of the growing front decreases as is the case if the front is assumed to be elliptic with the largest semi-axis in the x-direction. The mode III energy release rate has also been computed by (1) and the numerical results (not shown) display a similar sensitivity to the shape of the front at $\alpha = 0°$. For a circular front the mode III energy release rate remains below $G_0/5$ at stress levels below $\sigma/\sigma_c = 8$, and it is only significant very close to $\alpha = 0°$. Typically, the mode III energy release rate results in a contribution to interface fracture criteria, which is less than $1/6$ of its value (Jensen et al., 1990). By this and the observation that the peak value of G_{III} is very localised and considerably lower than $G_{\text{I/II}}$ it seems reasonable to neglect load-path dependent effects associated with the mode III component in the fracture criterion.

The peak value of the energy release rate that occurs in the transition region between the straight sides ($0 < s/b < 3$) and the semi-circular crack front ($3 < s/b < 4.57$) is illustrated in Fig. 4. Here, G is shown as a function of the location along the crack front at three stress levels. Sufficiently far behind the propagating front the numerical results can be compared with the exact result (9) (see Jensen and Sheinman, 2001). In the semi-circular front it is seen that there are only minor variations of G on the part of the front facing the direction of propagation (say $3.79 < s/b < 4.57$ corresponding to $45° < \alpha < 90°$), which is also evident from Fig. 3. Included in Fig. 4 is a typical finite element mesh used for the delaminated region resulting in 960 degrees of freedom.

The accuracy of the finite element calculations of $G(\alpha)$ shown in Fig. 3 is demonstrated in Fig. 5, where a comparison of G_{ss} and $\int_{0°}^{90°} G(\alpha)\sin\alpha\,\mathrm{d}\alpha$ has been shown. The result for G_{ss} in (9) is exact independent of the shape of the growing crack front. So the integral along the front of the local energy release rate $G(\alpha)$ projected on to the direction of growth should be equal to G_{ss} for any shape. The result for the circular front in Fig. 5 is close to G_{ss} and also numerical results obtained for different elliptic shapes of the front converge towards G_{ss} as the mesh size is decreased.

The actual shape of the growing front should be one where the fracture criterion is satisfied locally everywhere along the crack front. A family of fracture criteria formulated in Jensen et al. (1990) is given by

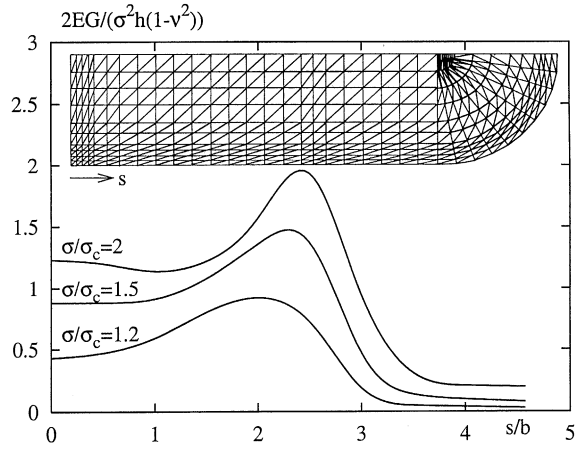

Fig. 4. Variation along the crack front of energy release rate at three stress levels. A finite element mesh resulting in 960 degrees of freedom is included.

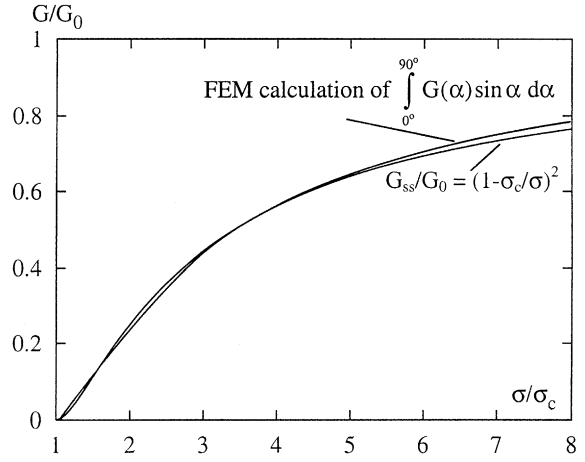

Fig. 5. Comparison of average energy release rate along the circular front with the exact result for G_{ss} (9).

$$G = G_{\mathrm{I,c}}\left(1 + (\lambda_2 - 1)\sin^2\psi\sin^2\phi + (\lambda_3 - 1)\cos^2\phi\right)^{-1} \tag{11}$$

with $\lambda_{2,3}$ being factors between 0 and 1 adjusting the contribution of modes II and III to the fracture criterion, and $G_{\mathrm{I,c}}$ is the mode I fracture toughness. While Jensen et al. (1990) allowed the shape of the crack front to be arbitrary and determined so that (11) was satisfied locally along the crack front, we in this work have chosen to compare different elliptic shapes of the propagating front. As discussed above the mode III contribution to (11) can be neglected since $85° < \phi < 90°$, and (11) reduces to

$$G = G_{\mathrm{I,c}}\left(1 + (\lambda_2 - 1)\sin^2\psi\right)^{-1} \quad \text{or} \quad K_{\mathrm{I}} = \sqrt{\frac{EG_{\mathrm{I,c}}}{1-\nu^2}} \quad \text{for } \lambda_2 = 0 \tag{12}$$

In Fig. 6 the finite element results for the variation of ψ at increasing stress levels is shown at two points along the growing, circular front: $\alpha = 0°$ and $90°$ with α defined in Fig. 2. Included in Fig. 6 are the exact

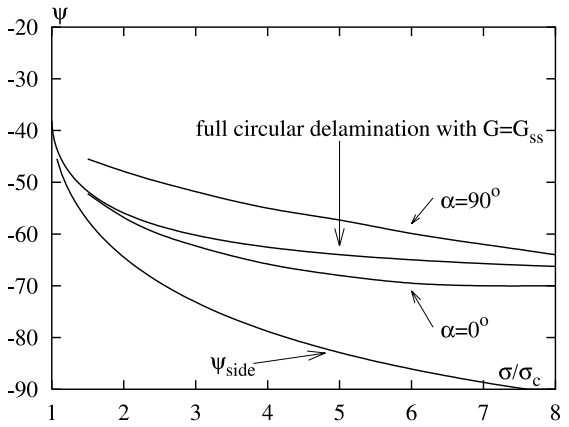

Fig. 6. Variation of phase angle of loading with increasing residual stresses shown at two locations along a circular crack front. Included for comparison is the estimate of ψ based on the full circular delamination and the phase angle of loading on the sides of a straight-sided delamination.

results, ψ_{side}, for the straight-sided delamination obtained by combination of (7) and (2). Also included are the results of the scheme proposed in Choi et al. (1999) for estimating ψ, which is to take the numerical results for a full circular delamination of radius b and re-scale the stress so that the energy release rate is equal to G_{ss}.

The results for the full circular delamination is obtained by numerical integration of the non-linear von Karman equations assuming axi-symmetric deformation

$$\begin{aligned}&\frac{\mathrm{d}^2}{\mathrm{d}r^2}\left(r\frac{\mathrm{d}^2w}{\mathrm{d}r^2}\right)-\frac{\mathrm{d}^2w}{\mathrm{d}r^2}\left(\frac{rb^2 12(1-\nu^2)}{Eh^3}N+\frac{1}{r}\right)-\frac{\mathrm{d}w}{\mathrm{d}r}\left(\frac{b^2 12(1-\nu^2)}{Eh^3}\left(\frac{\mathrm{d}(rN)}{\mathrm{d}r}\right)-\frac{1}{r^2}\right)=0\\&\frac{h^2}{6(1-\nu^2)}\frac{\mathrm{d}}{\mathrm{d}r}\left(r^3\frac{\mathrm{d}N}{\mathrm{d}r}\right)+r\left(\frac{\mathrm{d}w}{\mathrm{d}r}\right)^2=0\end{aligned}\tag{13}$$

The boundary conditions are given by assuming that the delaminated region is clamped to the substrate along the crack front

$$w=0,\quad \frac{\mathrm{d}w}{\mathrm{d}r}=0,\quad \frac{\mathrm{d}}{\mathrm{d}r}(rN)-\nu N+(1-\nu)\sigma h=0\tag{14}$$

and the continuity conditions at $r=0$ can be stated as

$$\frac{\mathrm{d}w}{\mathrm{d}r}=0,\quad \frac{\mathrm{d}^3w}{\mathrm{d}r^3}=0,\quad \frac{\mathrm{d}N}{\mathrm{d}r}=0\tag{15}$$

The energy release rate and the phase angle of loading is calculated by (1) and (2) using discontinuities across the crack front of N and $M=Eh^3/(12(1-\nu^2))(\mathrm{d}^2w/\mathrm{d}r^2)$.

The results in Fig. 6 show that the simple estimate of ψ is sufficiently accurate: it lies between the extreme values at $\alpha=90°$ and 0°, and by comparison of Figs. 3 and 5 it is seen that there is less variation of ψ with α than the variation of G with α. Furthermore, the loading close to $\alpha=0°$ is more mode II dominated than close to $\alpha=90°$ which compensates for the higher values of G close to $\alpha=0°$.

The shape of the growing crack front depends on the stress level and the interface fracture criterion. Assume a fracture criterion based on the mode I stress intensity factor (Eq. (12) for $\lambda_2=0$) so that the shape of the growing front should have a constant value of K_{I} along the front. Among the various elliptic

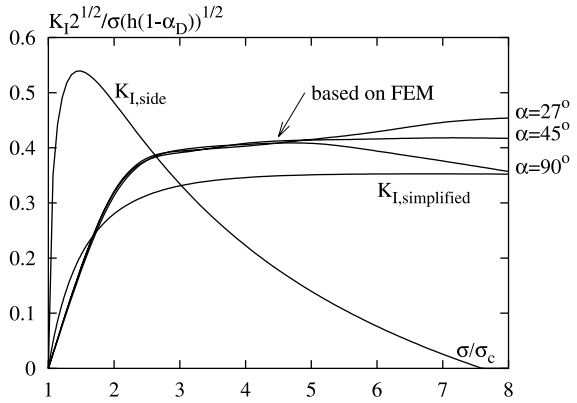

Fig. 7. Variation of mode I stress intensity factor with increasing residual stresses shown at different locations along a circular crack front.

shapes investigated numerically, the circular shape of the propagating front results in the smallest variation of K_I along the crack front. In Fig. 7 the variation of the normalised mode I stress intensity factor is shown at three points along the front ($\alpha = 27°$, 45° and 90°). The variation of K_I between these three points is very small. Included in Fig. 7 is the value $K_{I,side}$ along the straight-sided delamination and the value of K_I predicted from the simplified scheme combining ψ for the full circular delamination with G_{ss}.

In Fig. 7 it is seen that the circular shape of the growing crack front results in a nearly constant mode I stress intensity factor along the crack front for normalised stresses up to roughly $\sigma/\sigma_c = 5$. As shown in Jensen and Sheinman (2001) a secondary bifurcation buckling of the delaminated region due to the residual stresses occurs at $\sigma/\sigma_c = 5.6$, which by comparison with Fig. 6 is the stress level where the mode I stress intensity factors at different locations along the propagating front begin to deviate. Closer to $\alpha = 0°$ than shown in the figure, some deviations of K_I are seen but this is not believed to be significant. The stress intensity factor based on the simplified scheme slightly underestimates the value based on the finite element calculations but it is more accurate than might be expected. The mode I stress intensity factor along the crack front exceeds the stress intensity factor along the sides of the delamination indicating that growth of the front is favoured over growth along the sides for $\sigma/\sigma_c > 2.5$. This is a condition of consistency that has to be satisfied in order for steady-state buckling-driven delamination to be possible.

For other interface fracture criteria than the mode I criterion in (12) or at higher stress levels than $\sigma/\sigma_c = 5$ the shape of the growing front will no longer be circular. A further investigation of the dependence of the shape on the stress level and the interface fracture criterion is not carried out.

5. Steady-state delamination growth along circular paths

Assume a delamination propagating along a circular path and with circular sides of outer radius R_{ou} and inner radius $R_{ou} - 2b$ as sketched in Fig. 8. Assuming that the energy released during delamination growth is load-path independent the energy release rate along the growing front, G_{ss}, is

$$G_{ss}2b(R_{ou} - b) = \int_0^{2b} \left[G_{ou}(\tilde{b})R_{ou} + G_{in}(\tilde{b})(R_{ou} - 2\tilde{b}) \right] d\tilde{b} \tag{16}$$

where the energy release rate along the inner and outer sides of the delamination is denoted G_{in} and G_{ou}. The energy release rate along the circular sides of the delamination may be obtained by a simplified analysis

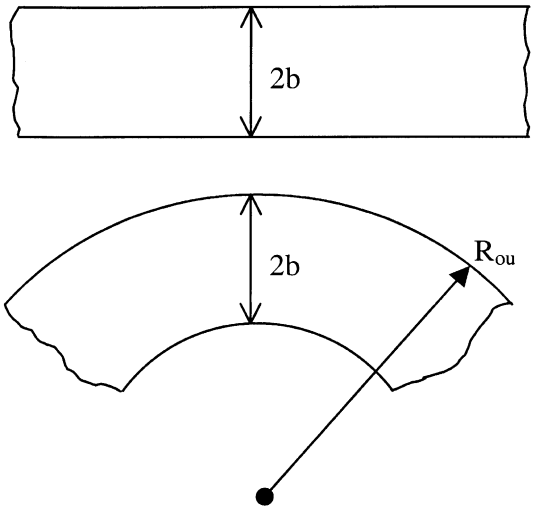

Fig. 8. Illustration of delaminations growing along straight-sided and circular paths.

where axi-symmetric deformation far behind the growing front is assumed. Thus, by Eq. (16) G_{ss} can be calculated without having to resolve the complex stress state along the growing front of delamination, precisely as for the case of growth along a linear path.

The previous section showed that estimating the phase angle of loading by re-scaling the results for a full circular delamination is sufficiently accurate for the straight-sided mode of delamination. This estimate of ψ is in the following assumed to be accurate also for growth along circular paths. Delaminations of identical widths growing along different circular paths have the same phase angle of loading, and a comparison can be based solely on G_{ss}.

The stress state far behind the propagating front is axi-symmetric so the governing equations for deformation of the delaminated region is given by (13). Both sides are clamped so (14) applies on the inner and the outer side. At first the governing Eqs. (13) and (14) are integrated numerically using a multiple shooting method and then (16) is integrated numerically.

In the numerical integrations a new parameter shows up when comparing the results for G_{ss}, which is the initial value of $2b$ when bifurcation buckling of the delaminated region occurs. Two examples of the results based on numerical integration of (16) compared with the exact result for G_{ss} (9) for a straight-sided delamination are shown in Fig. 9, one with $2b = 0.5R_{ou}$ at bifurcation and one with $2b = 0.4R_{ou}$. The initial value of $2b$ has a minor significance on the bifurcation stress, and for $2b = R_{ou}$ at bifurcation good agreement with the bifurcation stress in Evans and Hutchinson (1984) is obtained for a circular delamination pinned to the substrate at the centre. A value $v = 1/3$ has been used in the calculations, but the value has minor influence on the results. The integration of (16) is in both cases carried out with $2b$ varying from its initial specified value to $2b = R_{ou}$ where the radius of the inner side becomes 0 (see Fig. 8). The point $2b = R_{ou}$ is marked in Fig. 9 for both values of initial curvatures at bifurcation, the highest value of the normalised stress σ/σ_c corresponds to the highest value of $2b$ by (8). There is no method for calculating the initial value of $2b$ at bifurcation buckling and in practical applications it must depend on initial imperfections and defects in the system. By the results in Fig. 9, however, it is seen that for each value of initial curvature at bifurcation, the highest value of G_{ss} is obtained by integrating (16) to $2b = R_{ou}$. By Fig. 9 it is also seen that in general at small stress levels, the steady-state energy release rate for growth along a linear path is higher than that required for growth along a curved path. At higher stress levels, the curved path

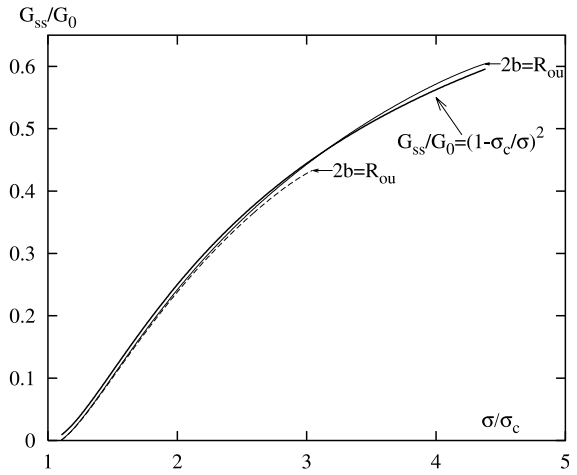

Fig. 9. Steady-state energy release rate for growth along two circular paths compared to the energy release rate for straight-sided delamination (9). The lower curve terminating at $\sigma/\sigma_c = 3.1$ where $2b = R_{ou}$ corresponds to $2b = 0.4R_{ou}$ at bifurcation. The upper curve terminating at $\sigma/\sigma_c = 4.4$ where $2b = R_{ou}$ corresponds to $2b = 0.5R_{ou}$ at bifurcation.

releases more energy than the linear path. The most likely mode to be observed would be expected to be that releasing most energy stored in the film.

In Fig. 10 the results for G_{ss} obtained for each initial curvature of delamination are shown by integrating (16) to $2b = R_{ou}$. The results are compared to the exact result in (9) for straight-sided delamination. At low stress levels the straight-sided delamination is most likely to be observed, but the curved delamination releases more energy at higher stress levels.

The asymptotic value of G_{ss} for the straight-sided delamination at infinitely high stresses where the film is completely delaminated is G_0. A full circular delamination has G_1 as an asymptotic value for the energy release rate at infinitely high stress levels corresponding to all the stored energy in the film being released.

The inset in Fig. 10 shows a schematic illustration of buckling-driven delamination growth along a circular path with $2b = R_{ou}$. The delamination can grow a finite distance, only, before the delaminated

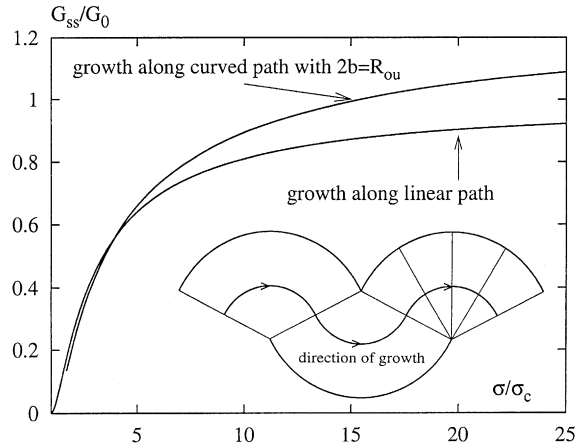

Fig. 10. Steady-state energy release rate for growth along a circular path with $2b = R_{ou}$ compared to the energy release rate for straight-sided delamination (9). Possible growth along a curved path with $2b = R_{ou}$ is illustrated.

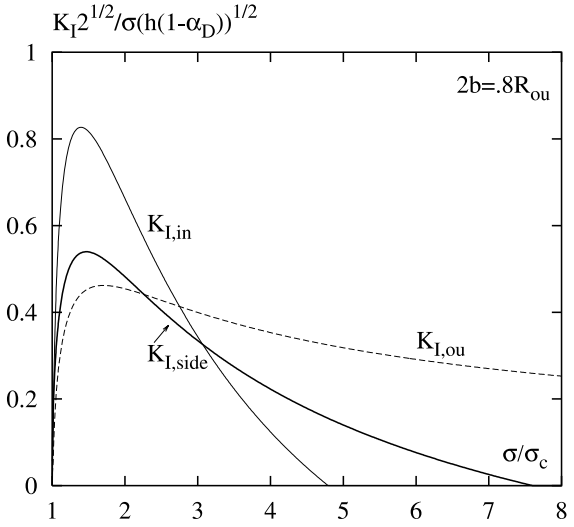

Fig. 11. Mode I stress intensity factors along the curved sides of delamination compared to the value on the straight-sided delamination.

region affects the growing front, at which point the growth direction would shift. This growth pattern would then be repeated. The energy required for the delamination to change its growth direction is not estimated in the present analysis.

Finally, it is verified that the buckling-driven delamination growing in a curved path satisfies the same consistency conditions as the straight-sided delamination evident from Fig. 7: the energy release with the effect of the phase angle of loading included must be higher on the growing front than the sides behind the front. In Fig. 11 the mode I stress intensity factor along the circular sides in the case $2b = 0.8R_{ou}$ is shown at increasing stress levels. The results are typical: K_I has a higher peak on the inner side of delamination but crack closure occurs on this side sooner than the straight-sided delamination. By comparing to K_I on the growing front shown in Fig. 7 it is seen that K_I on both sides of the delamination is lower. The only exception to this is K_I on the inner side on very low stress levels as $2b \to R_{ou}$. In that limit, however, the fundamental assumption of the curvature of the crack front being small compared to the film thickness breaks down. It should then be expected that unloading due to converging debonds as discussed in He et al. (1997) applies and as a result, the predictions of G_{ss} on the curved path are consistent in the sense that growth along the front is favoured over growth at the sides.

6. Conclusion

Numerical results based on the finite element method have been obtained for the phase angle of loading on the front of buckling-driven delamination growing along a linear path. The results are in very good agreement with an approach that has been suggested based on a re-scaling of the phase angle of loading for a full circular delamination. It has been shown that the shape of the growing crack front is best approximated by a semi-circle amongst the various elliptic shapes which have been compared. This, however, is true only at moderate stress levels when a mode II independent interface fracture criterion is assumed and the shape of the front has not been determined at higher stress levels and for other fracture criteria. The

simplified approach for estimating the phase angle of loading slightly underestimates the mode I stress intensity factor on the crack front. As a result, the range of stresses where growth along the front is favoured over growth along the sides is larger than predicted with the simple model.

A comparison of the energy release rate for delaminations growing along circular paths has been carried out. The results show that growth along a straight line is most likely to be observed at low stress levels while growth along curved paths are more likely at higher stresses. The mode of delamination that releases most energy at high stress levels has the centre of the circular path on one of the sides.

Acknowledgements

The work of I.S. was carried out during a stay as Visiting Professor at the Department of Solid Mechanics, Technical University of Denmark supported by the Danish Research Academy. The work of H.M.J. was supported in part by the Danish Research Agency under grant 9901360 (Materials Research) and in part by the EFP-2001 research programme on scale effects in design with composites.

References

ADINA, 1994. ADINA Users Manual. ADINA R&D, Watertown, MA USA.

Cao, H.C., Evans, A.G., 1989. An experimental study of the fracture resistance of bimaterial interfaces. Mechanics of Materials 7, 295–304.

Choi, S.R., Hutchinson, J.W., Evans, A.G., 1999. Delamination of multilayer thermal barrier coatings. Mechanics of Materials 31, 431–447.

Dundurs, J., 1969. Edge-bonded dissimilar orthogonal elastic wedges. Journal of Applied Mechanics 36, 650–652.

Evans, A.G., Hutchinson, J.W., 1984. On the mechanics of delamination and spalling in compressed films. International Journal of Solids and Structures 20, 455–466.

Gille, G., Rau, B., 1984. Buckling instability and adhesion of carbon layers. Thin Solid Films 120, 109–121.

Gioia, G., Ortiz, M., 1996. Delamination of compressed thin films. Advances in Applied Mechanics 33, 119–192.

He, M.Y., Evans, A.G., Hutchinson, J.W., 1997. Convergent debonding of films and fibers. Acta Materialia 45, 3481–3489.

Hutchinson, J.W., 2000. Delamination of compressed films on curved substrates. Harvard University Report, Mech 366.

Hutchinson, J.W., Suo, Z., 1992. Mixed mode cracking in layered materials. Advances in Applied Mechanics 29, 63–191.

Hutchinson, J.W., He, M.Y., Evans, A.G., 2000. The influence of imperfections on the nucleation and propagation of buckling driven delaminations. Journal of the Mechanics and Physics of Solids 48, 709–734.

Iyer, S.B., Harshavardhan, K.S., Kumar, V., 1995. Buckling patterns in diamond-like carbon films. Thin Solid Films 256, 94–100.

Jensen, H.M., 1993. Energy release rates and stability of straight-sided, thin-film delaminations. Acta Materialia 41, 601–607.

Jensen, H.M., Sheinman, I., 2001. Straight-sided, buckling-driven delamination at high stress levels. International Journal of Fracture 110, 371–385.

Jensen, H.M., Hutchinson, J.W., Kim, K.-S., 1990. Decohesion of a cut prestressed film on a substrate. International Journal of Solids and Structures 26, 1099–1114.

Matuda, N., Baba, S., Kinbara, A., 1981. Internal stress, Young's modulus and adhesion energy of carbon films on glass substrates. Thin Solid Films 81, 301–305.

Ogawa, K., Ohkoshi, T., Takeuchi, T., Mizoguchi, T., Masumoto, T., 1986. Nucleation and growth of stress relief patterns in sputtered molybdenum films. Japanese Journal of Applied Physics 25, 695–700.

Ortiz, M., Gioia, G., 1994. The morphology and folding patterns of buckling-driven thin-film blisters. Journal of the Mechanics and Physics of Solids 42, 531–559.

Rice, J.R., 1988. Elastic fracture mechanics concepts for interfacial cracks. Journal of Applied Mechanics 55, 98–103.

Sergo, V., Clarke, D.R., 1998. Observation of subcritical spall propagation of a thermal barrier coating. Journal of the American Ceramic Society 81, 3237–3242.

Stringfellow, R.G., Freund, L.B., 1993. The effect of interfacial friction on the buckle-driven spontaneous delamination of a compressed thin film. International Journal of Solids and Structures 30, 1379–1395.

Suo, Z., Hutchinson, J.W., 1990. Interface crack between two elastic layers. International Journal of Fracture 43, 1–18.
Thouless, M.D., 1993. Combined buckling and cracking of films. Journal of the American Ceramic Society 76, 2936–2938.
Thouless, M.D., Hutchinson, J.W., Liniger, E.G., 1992. Plane-strain, buckling-driven delamination of thin films: model experiments and mode II fracture. Acta Materialia 40, 2639–2649.
Wang, J.-S., Evans, A.G., 1998. Measurement and analysis of buckling and buckle propagation in compressed oxide layers on superalloy substrates. Acta Materialia 46, 4993–5005.